Advances in Geo-Energy Research

Vol. 11, No. 2, p. 152-160, 2024

Original article

Petrophysical recipe for in-situ CO_2 mineralization in basalt rocks

Yongqiang Chen[1,2]*, Mojtaba Seyyedi[1,2,3], Ben Clennell[1]

[1]*Energy BU, CSIRO, Kensington, WA 6151, Australia*
[2]*Permanent Carbon Locking Future Science Platform, CSIRO, Australia*
[3]*(Current) Global CCS Institute, Docklands, VIC 3008, Australia*

Keywords:
In-situ CO_2 mineralization
basalt rocks
mafic and ultramafic minerals
optimal petrophysical conditions
geochemical modelling

Cited as:
Chen, Y., Seyyedi, M., Clennell, B. Petrophysical recipe for in-situ CO_2 mineralization in basalt rocks. Advances in Geo-Energy Research, 2024, 11(2): 152-160.
https://doi.org/10.46690/ager.2024.02.07

Abstract:
In-situ carbon dioxide mineralization in basalt rocks has been identified as a scalable, fast, safe, permanent, and cost-effective method to offset the anthropogenic carbon dioxide emissions. In-situ carbon dioxide mineralization refers to underground carbon dioxide transformation to carbonate minerals in basalt reservoirs. Although current field applications achieved fast in-situ carbon dioxide mineralization, limited petrophysical criteria have been proposed to screen a potential site to implement in-situ carbon dioxide mineralization. To fill this knowledge gap, geochemical modellings were performed to find an optimal petrophysical recipe, including pressure, temperature, pH, and mineral composition, to conduct in-situ carbon dioxide mineralization. The geochemical modellings showed that increasing pressure was favourable to increase water uptake of carbon dioxide, host rock dissolution, and in-situ carbon dioxide mineralization. However, a higher temperature depressed the in-situ carbon dioxide mineralization. Furthermore, the in-situ carbon dioxide mineralization was unravelled to be heavily pH dependent. Most magnesite precipitated in pH range from 9 to 11. Moreover, the forsterite was identified as the major contributing minerals while anorthite, fayalite, and diopside played a minor role in the in-situ carbon dioxide mineralization. This investigation provided a general protocol to screen the optimal petrophysical conditions for in-situ carbon dioxide mineralization.

1. Introduction

To achieve net-zero goal by 2050, at least 107 Gt carbon dioxide (CO_2) is required to be removed from air (data from IEA Clean Technology Scenario (Agency, 2019)). Surface storage of such amount of CO_2 is a significant challenge. Underground CO_2 storage is thus put forward to mitigate the anthropogenic greenhouse gas emissions. CO_2 captured from direct air capture or large point source emitters (e.g., coal power plants) is injected into underground reservoirs for permanent storage (Chen et al., 2021, 2023; Zhong et al., 2023).

Conventional CO_2 geological storage mainly holds CO_2 in saline formations (Bentham and Kirby, 2005; Michael et al., 2009; Bachu, 2015) and depleted oil and gas reservoirs. The conventional CO_2 geological storage keeps CO_2 underground by four major mechanisms: 1) residual trapping (capillary force immobilizes CO_2 ganglions in pores) (Saeedi et al., 2012); 2) structural trapping (caprock blocks upward CO_2 migration by high capillary entry pressures) (Bradshaw et al., 2007; Nilsen et al., 2012; Gasda et al., 2013); 3) dissolution trapping (CO_2 dissolves in brine) (Anchliya et al., 2012; Agartan et al., 2015; Soltanian et al., 2017; Chen et al., 2018); and 4) mineral trapping (or geochemical trapping, CO_2 converts to minerals) (Underschultz et al., 2011; Hannis et al., 2017; Pearce et al., 2022a, 2022b). Although large amount of CO_2 can be injected into underground reservoirs (Bradshaw et al., 2007), most CO_2 exists in a liquid or supercritical status, which is not stable and is likely to leak to surface. To mitigate this leakage risk, in-situ CO_2 mineralization method was thus proposed, where the CO_2 is injected into highly reactive

Yandy Scientific Press

*Corresponding author.
E-mail address: yongqiang.chen@csiro.au (Y. Chen); mojtaba.seyyedi@globalccsinstitute.com (M. Seyyedi); ben.clennell@csiro.au (B. Clennell).

Received December 18, 2023; revised January 7, 2024; accepted January 25, 2024; available online January 29, 2024.

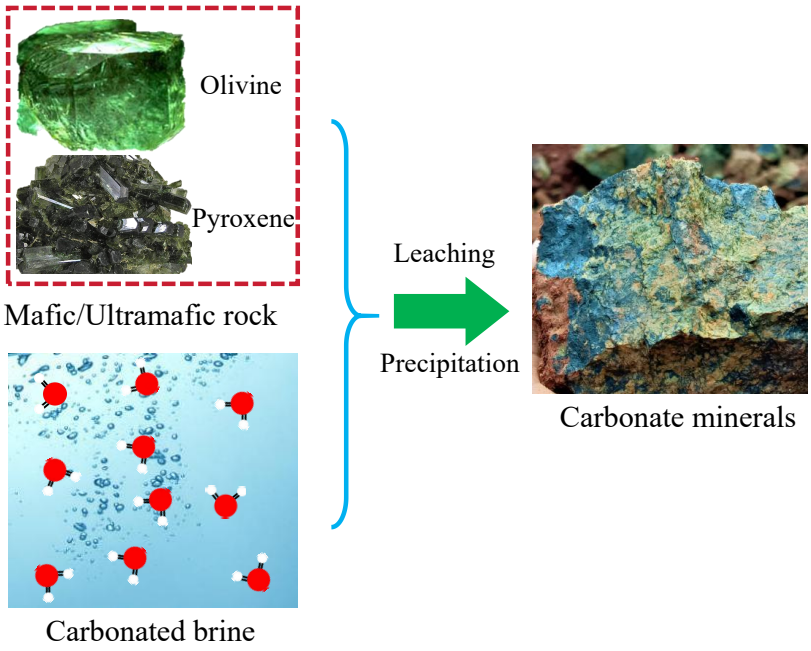

Fig. 1. Schematic graph of in-situ "carbon locking" process.

basaltic rocks to convert the gaseous CO_2 to inactive solid carbonate minerals.

The basalt rocks include mafic and ultramafic minerals, which can be magnitudes more reactive than the conventional sandstone rocks (Schaef et al., 2011). This character enables a rapid in-situ CO_2 conversion to carbonate minerals. This rapid in-situ CO_2 mineralization in mafic and ultramafic rocks can be achieved through two key processes: host rock leaching and carbonate mineral precipitations (as shown in Fig. 1) (Raza et al., 2022). In the leaching process, the reactive minerals (especially Ca, Mg, and Fe bearing minerals) dissolve and release cations once exposed to acidic CO_2-rich brine. This leaching process is much faster than the natural weathering due to the vulnerable character of mafic and ultramafic rocks in acidic CO_2-rich brine (Hartmann et al., 2013). The leached cations (Ca^{2+}, Mg^{2+}, and Fe^{2+}) then combine with the CO_3^{2-} to form the carbonate precipitations and thus achieve in-situ CO_2 mineralization (Kanakiya et al., 2017).

The fast leaching is crucial to achieve efficient in-situ CO_2 mineralization. As Goldich dissolution series predicted, the dissolution rate of mafic and ultramafic rocks follows a sequence of olivine, pyroxene, amphibole, and biotite. For example, the forsterite (a family member of olivine) dissolution rate can reach over 10^{-12} mol/cm^2/s (from Oelkers et al. (2018)). This fast dissolution accelerates cations releasing for subsequent formation of carbonate minerals. In addition to dissolution reaction, serpentinization releases cations from host rock to aqueous phase. The serpentinization produces Ca^{2+}, Mg^{2+}, and Fe^{2+} through hydrolysis reaction at low-temperature (Klein et al., 2013), which combine with CO_3^{2-} to form carbonate minerals. Collectively, in the carbonated brine, the dissolution and serpentinization reactions weaken the host mafic rocks and promote fast cation leaching. The leached cations, including Ca^{2+}, Mg^{2+}, and Fe^{2+} (and Fe^{3+}), combine with CO_3^{2-} to form carbonate minerals, which enables permanent in-situ CO_2 mineralization.

Fast in-situ CO_2 mineralization was reported to accomplish in basalt reservoirs within 2-4 years, such as the CarbFix project and Wallula Basalt Pilot Project. Specifically, the CarbFix project reported a substantially fast in-situ CO_2 mineralization in Iceland (Gunnarsson et al., 2018; Pogge von Strandmann et al., 2019). A total of 165 $\pm$ 8.3 t CO_2 was mineralized, 93% dissolved Ca was precipitated as calcite, and 72 $\pm$ 5% injected carbon was mineralized within two years (Pogge von Strandmann et al., 2019). Wallula Basalt Project injected supercritical CO_2 into the Columbia River Basalt Group (McGrail et al., 2014). The Columbia River Basalt Group is one of the best-preserved continental flood basalt provinces on Earth. They estimated that 10-50 Gt CO_2 can be converted to minerals in the Miocene Columbia River Basalt Group (McGrail et al., 2014). They proved the feasibility to implement the in-situ CO_2 mineralization in the continental flood basalt, which can extend the application to in-situ CO_2 mineralization in India, U.S. and Australia. In addition, the 44.01 project started commercial CO_2 injection in periodate rocks in Oman in 2023. Kelemen and Matter (Kelemen and Matter, 2008) estimated that carbonating CO_2 with only 1 wt% periodate in Oman would lock 25% of all atmospheric CO_2, which is almost the increased amount of CO_2 since industrial revolution. Collectively, current projects proved that fast and secure in-situ CO_2 mineralization is feasible in basalt formations.

Knowledge gaps and operational risks still exist in large-scale in-situ CO_2 mineralization. Firstly, current research has not determined an effective petrophysical recipe to implement in-situ CO_2 mineralization. For example, the effects of temperature and pressure have not been evaluated for their role in in-situ CO_2 mineralization. Secondly, the kinetics of host

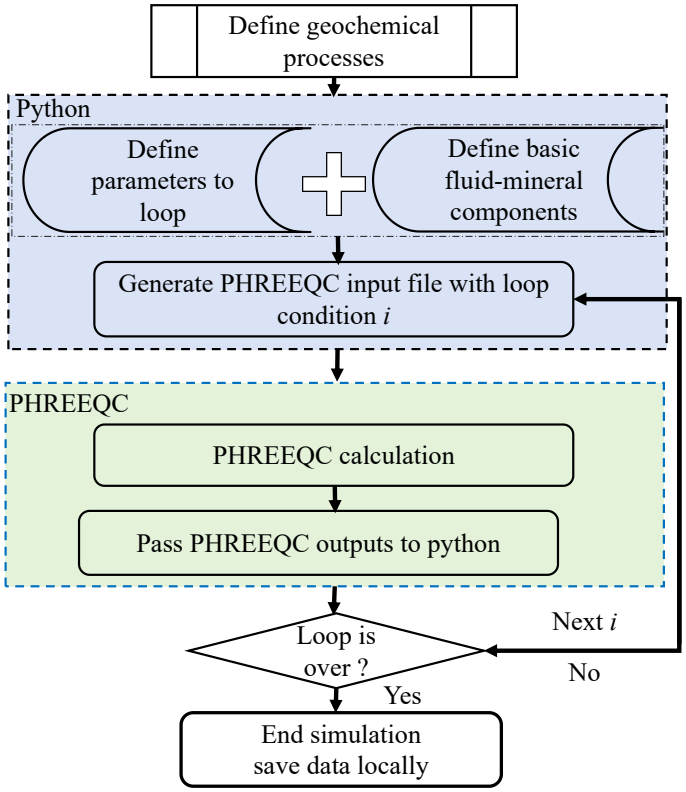

Fig. 2. Schematic diagram for coupling PHREEQC and Python to batch model the in-situ CO_2 mineralization under various temperature and pressure conditions.

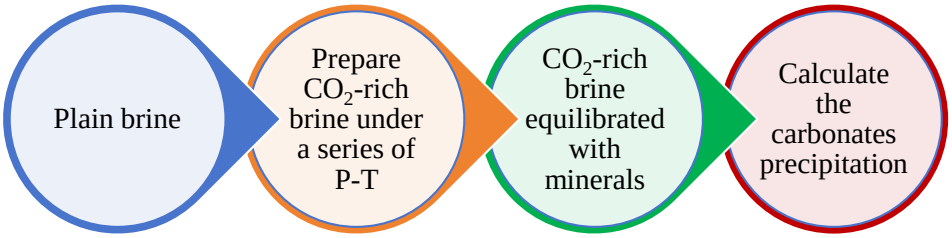

Fig. 3. Procedure to batch model the in-situ CO_2 mineralization (plain brine refers to the non-carbonated brine).

rock leaching and carbonate precipitation have not been well understood. The kinetic in-situ CO_2 mineralization has not been delineated at time scale. Thirdly, due to the dissolution of minerals, the dynamic evolution of fluid chemistry (e.g., pH) can yield various carbonate minerals. However, limited evaluation was performed to understand this process. To mitigate the potential risks and standardize the operation procedure, this investigation aims to find an effective petrophysical recipe to implement the in-situ CO_2 mineralization, including temperature, pressure, kinetics, pH, and brine compositions.

2. Methodology

2.1 Model description and assumptions

To model the in-situ CO_2 mineralization, a series of equilibrium reactions (batch reactions) were set up to evaluate the carbonate precipitations under multiple temperature and pressure conditions. The PHREEQC (Charlton and Parkhurst, 2011) (version: IPhreeqcCOM-3.7.3-15,968) was coupled with Python (version 3.9.13 distributed with Anaconda). In this coupling, the PHREEQC was the chemical reaction engine while the Python facilitated the iterations over temperature and pressure conditions (Fig. 2). The PHREEQC can simulate the batch reactions at a specific temperature and pressure. However, the built-in looping capacity in the PHREEQC is limited with I/O (input/output) capacity. Python was thus coupled to assist the batch modelling with its full looping and file operation capacities.

To evaluate the in-situ CO_2 mineralization at field scale, the batch modellings were prepared based on the procedure of field operation. As shown in Fig. 3, the in-situ CO_2 mineralization was modelled with three steps against the data from CarbFix project: 1) brine was equilibrated with CO_2 under the field temperature and pressure to obtain the CO_2 saturated brine, 2) the CO_2 saturated brine was equilibrated with host rock at the same field pressure and temperature,

Table 1. Geochemical reactions of in-situ CO_2 mineralization.

Reaction location/type	Mineral	Reaction	Log K
Host rock/dissolution	Albite	$NaAlSi_3O_8 + 4H^+ = Al^{3+} + Na^+ + 2H_2O + 3SiO_2$	2.7645
	Anorthite	$CaAl_2(SiO_4)_2 + 8H^+ = Ca^{2+} + 2Al^{3+} + 2SiO_2 + 4H_2O$	26.578
	Fayalite	$Fe_2SiO_4 + 4H^+ = SiO_2 + 2Fe^{2+} + 2H_2O$	19.1113
	Forsterite	$Mg_2SiO_4 + 4H^+ = SiO_2 + 2H_2O + 2Mg^{2+}$	27.8626
	Diopside	$CaMgSi_2O_6 + 4H^+ = Ca^{2+} + Mg^{2+} + 2H_2O + 2SiO_2$	20.9643
Aquifer/Mineral precipitation	Calcite	$CaCO_3 + H^+ = Ca^{2+} + HCO_3^-$	1.8487
	Magnesite	$MgCO_3 + H^+ = HCO_3^- + Mg^{2+}$	2.2936
	Brucite	$Mg(OH)_2 + 2H^+ = Mg^{2+} + 2H_2O$	16.298
	Siderite	$HCO_3^- + Fe^{2+} = FeCO_3 + H^+$	0.192
Aquifer/Carbonation	Carbonation	$HCO_3^- + H^+ = CO_2 + H_2O$	6.3447

Notes: The thermodynamic data are from Lawrence Livermore National Laboratory hermos.com.V8.R6.230 thermodynamic database.

and 3) the generation of carbonate minerals was calculated at equilibrium status. In the batch modellings, the rock/water volume ratio was 4:1 for a 20% porosity scenario. The same rock/water ratio applied to the kinetics modelling.

To evaluate the time-elapsed in-situ CO_2 mineralization, the generations of mineral species were evaluated through the kinetic calculations in PHREEQC. To be specific, the KINETICS and RATES module in PHREEQC were utilized to evaluate the dynamic dissolution and precipitation process. The mathematical equations of reaction rates were defined in the RATES module. The rate equations were then integrated over each time step with the Runge-Kutta algorithm. The kinetic calculation was facilitated by the BASIC library compiled by Zhang et al. (2019).

2.2 Batch geochemical reaction settings

To evaluate the host rock dissolution and carbonate precipitation, the dissolution reactions were modelled for the major minerals in mafic and ultramafic rocks, including plagioclase, fayalite (Fe_2SiO_4), and forsterite (Mg_2SiO_4). Given the albite ($NaAlSi_3O_8$) and anorthite ($CaAl_2Si_2O_8$) are sodium-rich and calcium-rich end members of plagioclase family, this model included the albite and anorthite to examine the effects of plagioclase in in-situ CO_2 mineralization. Furthermore, fayalite and forsterite are iron-rich and magnesium-rich end members of olivine family. To evaluate the effects of ultramafic rocks in in-situ CO_2 mineralization, fayalite and forsterite were included as the representative ultramafic minerals. The geochemical reactions were listed in Table 1.

2.3 Kinetic geochemical reaction settings

To model the dynamic mineralization process, a general rate equation was employed (as shown in Eqs. (1)-(4)). As indicated in the mathematical equation, the kinetics is a function of reactive surface area, species activity, activation energy, and saturation index. The reaction rates were from Palandri and Kharaka (2004). In this kinetic calculation, the reactive surface area was assumed to be 20 cm^2/kgw (kilogram water) (Aradóttir et al., 2012):

$$r_a = S_A A_{\mathrm{H}} e^{-E_{a,\mathrm{H}}/RT} a_{\mathrm{H}}^{n\mathrm{H}} (1-\Omega^{p_1})^{q_1} \quad (1)$$

$$r_w = S_A A_{\mathrm{H_2O}} e^{-E_{a,\mathrm{H_2O}}/RT} (1-\Omega^{p_2})^{q_2} \quad (2)$$

$$r_b = S_A A_{\mathrm{OH}} e^{-E_{a,\mathrm{OH}}/RT} a_{\mathrm{OH}}^{n\mathrm{OH}} (1-\Omega^{p_3})^{q_3} \quad (3)$$

$$r_n = r_a + r_w + r_b \quad (4)$$

where r_n is the net dissolution rate of a mineral phase, r_a is the mineral dissolution rate caused by H^+, r_w is the mineral dissolution rate caused by H_2O, r_b is the mineral dissolution rate caused by OH^-, S_A is the surface area of per unit water mass (m^2/(kgw)), A is the pre-exponential factor (mol/(m^2·s)), E_a is the activation energy (J/mol), T is the absolute temperature (K), a is the species activity, R is the ideal gas constant, Ω is the saturation index, p_1, p_2, p_3, q_1, q_2, and q_3 are dimensionless empirical parameters. The subscripts H, H_2O, and OH represent H^+, H_2O, and OH^-, respectively.

2.4 Input data from CarbFix field in-situ CO_2 mineralization project

To verify the fast in-situ CO_2 mineralization, the in-situ CO_2 mineralization process was calculated against the field observation data from CarbFix project. The rock composition was from Aradóttir et al. (2012) with 13% olivine, 43% plagioclase, 39% pyroxene, and 5% basalt glasses in weight, respectively. The olivine was composed of 20% fayalite and 80% forsterite. The plagioclase was composed of 30% albite and 70% anorthite. Diopside was the major component of pyroxene. All the information was extracted from Tables 3-4 of Aradóttir et al. (2012) and references therein.

To evaluate the effects of brine composition in in-situ CO_2

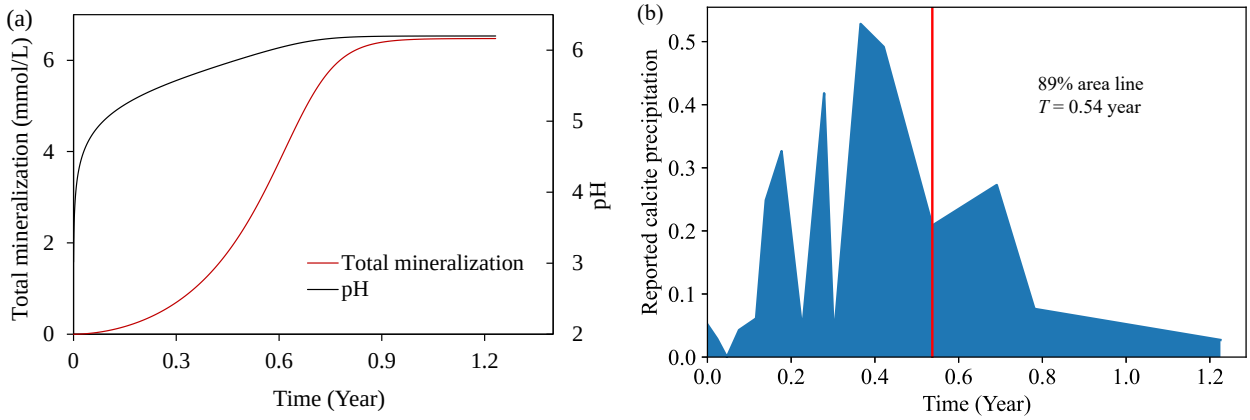

Fig. 4. Kinetics of in-situ CO_2 mineralization. (a) is the kinetic modelling of in-situ CO_2 mineralization with input petrophysical data from CarbFix project at the pressure of 1,469.5 psi and temperature at 25 °C; and (b) is the data retrieved and digitalized from Pogge von Strandmann et al. (2019), horizontal axis is time of the fluid sampling, vertical axis is the normalized calcite precipitation rate, the area in the left of the red line occupies 89% of the total area.

Table 2. Brine composition of CarbFix project (data from Well HN-01 in Table 1 of Pogge von Strandmann et al. (2019)).

Ion type	Na	Si	Ca	Sr	Li	pH
Concentration (ppm)	43.5	14.1	5.37	18.4	0.16	9.26

mineralization, the brine composition (in Table 2) reported from CarbFix project was used in the simulation. In the original CarbFix project, the brine from an aquifer was pumped out through the Well HN-01 and co-injected with CO_2 into target reservoirs through Well HN-02. In Well HN-01, the major cations were Na^+ and Sr^{2+} with a slight alkaline condition (pH = 9.26). Due to the absence of anion data, the Cl^- was assumed as the primary anion.

3. Results and discussion

3.1 Kinetics of in-situ CO_2 mineralization of CarbFix field pilot tests

To benchmark the geochemical model, the geochemical modelling results were compared with the field sampling data from CarbFix project. In the benchmark modellings, the amount of generated carbonate minerals was calculated by a kinetic geochemical modelling. The simulation results were compared with the reported calcite precipitation. The kinetic modellings in this study agreed well with the field sampling from CarbFix project. Both showed a fast in-situ CO_2 mineralization within 2 years (Fig. 4).

The data from Fig. 3 of Pogge von Strandmann et al. (2019) was digitalized and analysed, which was the calcite precipitation calculated from fluid sampling in CarbFix project. As shown in Fig. 4, the horizontal axis was the reaction time while the vertical axis was the mineralization rate. To get the amount of CO_2 precipitation, an integration was performed to get the area between the precipitation rate line and horizontal axis. A total amount of 89% of injected CO_2 was found to be mineralized at 0.54 year within the reservoir. Furthermore, at around 0.4 year of CO_2 injection, the in-situ CO_2 mineralization reached peak rate.

This kinetic modelling result was in line with the above field observations from CarbFix project. Both showed that the CO_2 can be mineralized in 1 year. In the kinetic modelling, the dynamic precipitation of carbonate minerals (e.g., $CaCO_3$, $FeCO_3$, and $MgCO_3$) was calculated. These kinetic simulations proved that 90% of CO_2 mineralization can be achieved in 0.9 year (Fig. 4). The brine pH increased from 3.5 at the beginning to 6.3 at the equilibrium, respectively. This kinetic simulation demonstrated that the maximal precipitation rate reaches at 0.6 year, which is close to the field observation (at 0.4 year). The slight difference could be due to the high percentage of basalt glass minerals in CarbFix reservoirs, the non-reactive transport of the batch modelling, or an enlarged surface area during the reactive transport flow.

3.2 Effect of temperature and pressure in in-situ CO_2 mineralization

The batch geochemical modelling was performed to find the "sweet spot" of temperature and pressure to accelerate the in-situ CO_2 mineralization. To evaluate the effect of pressure in CO_2 mineralization, the generation of $MgCO_3$, $FeCO_3$, and $CaCO_3$ was calculated in function of pressure. The mineral and fluid composition were from CarbFix project (Table 2). The generation of carbonate mineral was found to increase with increasing pressure for all three species (Fig. 5). To be specific, the generated $MgCO_3$ was the major carbonate mineral following by $FeCO_3$ and $CaCO_3$. For example, the $MgCO_3$ generation increased from 2.06×10^{-3} to 1.28×10^{2} mmol/L with pressure increasing from 0.01 to 826.4 psi. At the same pressure range, the $CaCO_3$ generation increased from 1.04×10^{-6} to 2.66×10^{-4} mmol/L. The increased carbonate mineral generation was due to the increased CO_2 uptake in the brine with increasing pressure. With increasing pressure, the CO_2 uptake in the brine increased, which generated more

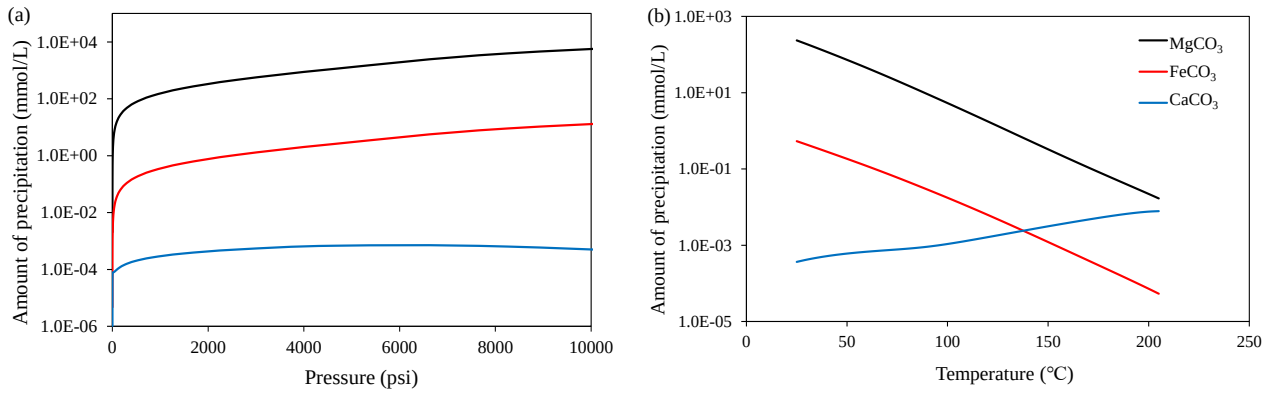

Fig. 5. Effect of pressure (a) and temperature (b) in mineral generations during in-situ CO_2 mineralization (based on field data from CarbFix project).

HCO_3^-. This reaction promoted the reaction HCO_3^- + Mg^{2+} = $MgCO_3$ + H^+ to the right and thus obtain more carbonate mineral precipitation. However, the mineral precipitation did not increase dramatically with pressure over 826.4 psi. This non-linear CO_2 water uptake vs pressure was due to the relation between CO_2 fugacity and pressure. The fugacity coefficient of CO_2 was calculated by PHREEQC with the Peng-Robinson equation of state. At high pressure, the fugacity coefficient of CO_2 dropped rapidly, which caused gradual increasing dissolved CO_2 concentration (see example 22 in Parkhurst and Appelo (2013)). This mineralization pathway indicated that 600 m is an optimal depth to implement in-situ CO_2 mineralization, where the cost for gas compression is low while the amount of in-situ CO_2 mineralized is not compromised substantially compared to deep wells.

To evaluate the effect of temperature in CO_2 mineralization, the generation of $MgCO_3$, $FeCO_3$, and $CaCO_3$ was calculated with increasing temperature. The $MgCO_3$ and $FeCO_3$ were found to decrease with increasing temperature. However, the generation of $CaCO_3$ increased with increasing temperature. The different responses to temperature can be explained by enthalpy changes of geochemical reactions. The enthalpy change of Ca^{2+} + HCO_3^- = $CaCO_3$ + H^+ is 30.5767 kJ/mol while the enthalpy change of Mg^{2+} + HCO_3^- = $MgCO_3$ + H^+ is -23.8279 kJ/mol (from LLNL thermodynamic database). This enthalpy change indicated that the generation of $CaCO_3$ was promoted by the increasing temperature while the generation of $MgCO_3$ was suppressed by increasing temperature (as shown in Fig. 5). However, the total amount of carbonate minerals generation decreased with increasing temperature, which indicated a lower reservoirs temperature would be favourable for the in-situ CO_2 mineralization.

3.3 Effect of pH in in-situ CO_2 mineralization

The pH played a critical role in the formation of carbonate minerals. The carbon species distribution was calculated to identify the major precipitated carbonates against pH. Fig. 5 indicated that the production of $MgCO_3$ was magnitude higher than $CaCO_3$ and $FeCO_3$. In Fig. 6, the pH affected concentration of $MgCO_3$ and other soluble carbon species were analysed in the aqueous solution. At pH < 4, most carbon species existed in the brine as free CO_2. With pH increasing from 4 to 7.69, the percentage of free CO_2 decreased while the HCO_3^- and $MgHCO_3^+$ increased to the peak percentage at 68.2% and 25.8%, respectively. Furthermore, at pH > 8, the percentage of $MgCO_3$ increased significantly from nearly 0 to 50.8% at pH = 10.6. Most precipitation of $MgCO_3$ was generated in pH between 8 and 11. This effect of pH in CO_2 mineralization was in line with literature observation. For example, Saldi et al. (2012) observed that the major magnesite precipitation occurred at pH > 7. Ji et al. (2022) found that increasing pH raised the activity of CO_3^{2-}, which promoted the transition of hydromagnesite to magnesite. The pH dependant character of in-situ CO_2 mineralization indicated that manipulating pH (or increasing alkalinity) can accelerate in-situ CO_2 mineralization in basalt reservoirs.

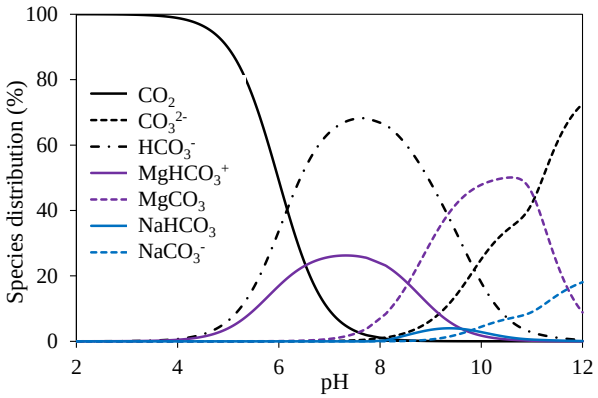

Fig. 6. Carbon species distribution versus pH (plotted with PhreePlot (Kinniburgh and Cooper, 2011)).

3.4 Effect of mineral composition in in-situ CO_2 mineralization

To evaluate the effects of each mineral composition in in-situ CO_2 mineralization, the amount of carbonate precipitation was calculated as a function of mineral compositions. Given that the albite does not release cations during leaching, the effects of active minerals with fayalite, forsterite, and diopside

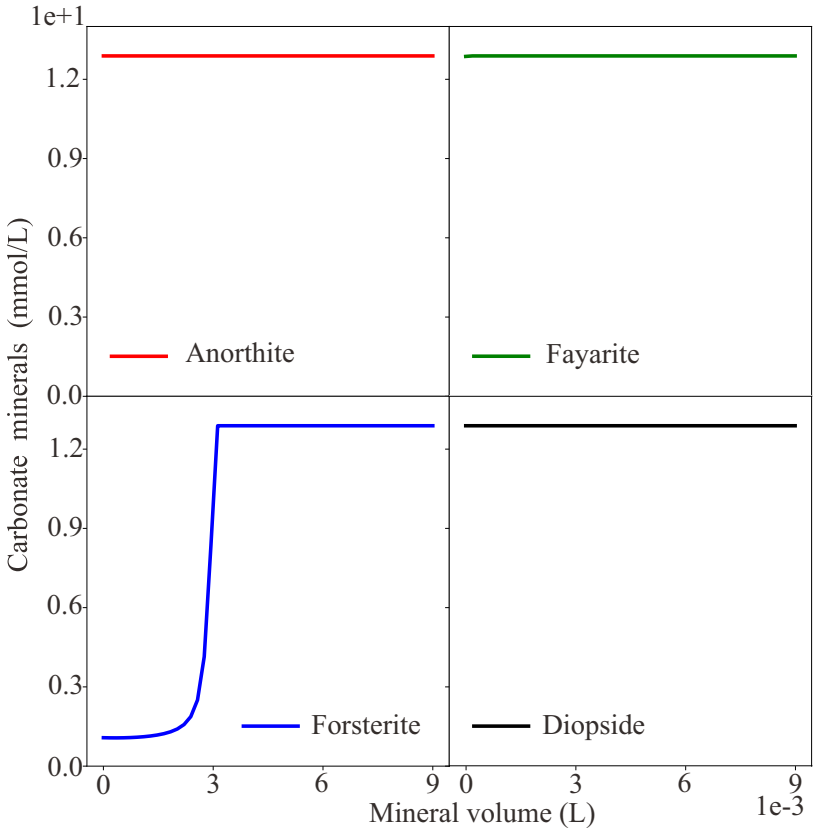

Fig. 7. Effect of mineral composition in in-situ CO_2 mineralization.

were estimated. In the analysis, the amount of carbonate minerals was calculated to evaluate the in-situ CO_2 mineralization. The volume of one mineral (e.g., fayalite) slightly increased from 0 to 0.01 L. At the same time, the total rock volume kept constant to achieve a fixed rock/water ratio. The constant rock volume was accomplished by correspondingly decreasing the volume of the non-contributing albite while keeping the volumes of other minerals constant. The rock/water ratio was one of the key parameters to affect CO_2-water-rock interactions (Rosenbauer et al., 2012), which was the reason to use constant rock/water ratio in the sensitivity simulations.

As shown in Fig. 7, the magnesium bearing forsterite was the primary mineral to convert the aqueous carbon (CO_3^{2-}) to magnesite ($MgCO_3$). With increasing volume of forsterite from 0 to 0.0029 L (equivalent to 0.068 mol), the total CO_2 precipitation increased from 1.08 to 8.37 mmol/L. However, other mineral compositions (e.g., anorthite, fayalite, and diopside) showed negligible effects in in-situ CO_2 mineralization. By increasing the volume of anorthite, fayalite, and diopside from 0 to 0.009 L, the amount of carbon mineralization increased less than 0.1 mmol/L. The total contribution of anorthite, fayalite, and diopside to mineralization can be approximated to 1.08 mmol/L when the amount of forsterite is 0. Considering that the maximal amount of mineralization can reach 12.89 mmol/L, the 1.08 mmol carbonate precipitation from anorthite, fayalite, and diopside approximately contributed 8.4% of total carbonate mineralization, which was a minor contribution to the in-situ CO_2 mineralization. This sensitivity analysis was consistent with Snæbjörnsdóttir et al. (2020). Their excellent review showed that the forsterite released Mg^{2+} faster than diopside and basalt glass (Fig. 3(b) of Snæbjörnsdóttir et al. (2020)). The leached Mg^{2+} then reacted with CO_3^{2-} to form magnesite precipitation.

4. Conclusion and implication

In-situ CO_2 mineralization is a promising technology to achieve fast carbon removal at large scale. However, the research of in-situ CO_2 mineralization is in its infancy. Establishing a petrophysical criterion is thus crucial to implement in-situ CO_2 mineralization at large scale. In this investigation, the geochemical modelling was benchmarked with field data from CarbFix project to determine an optimal petrophysical recipe to accelerate in-situ CO_2 mineralization. The role of pressure, temperature, pH, and mineral compositions was evaluated for generation of carbonate minerals, including $CaCO_3$, $MgCO_3$, and $FeCO_3$.

Increasing pressure accelerated the in-situ CO_2 mineralization. The $CaCO_3$ generation increased from 1.04×10^{-6} to 2.66×10^{-4} mmol/L with pressure increasing from 0.01 to 826.4 psi. However, the mineral generation did not increase dramatically with pressure over 826.4 psi. This indicated that the pressure increase did not significantly affect the in-situ CO_2 mineralization deeper than 600 m. With increasing temperature, the generation of $MgCO_3$ and $FeCO_3$ decreased while the formation of $CaCO_3$ increased. However, the total amount of carbonate minerals decreased with increasing tem-

perature. Thus, a colder basalt reservoir performs better for in-situ CO_2 mineralization.

Most in-situ CO_2 mineralization can be achieved at pH between 9 and 11. At pH $<$ 4, most carbon species existed in the aqueous as free CO2. With pH increasing to 7.69, free CO_2 transmitted to HCO_3^- and $MgHCO_3^+$. With pH ranging between 8 and 11, most carbon species precipitated as $MgCO_3$. pH between 8 and 11 is thus a favourable "pH window" for in-situ CO_2 mineralization. Moreover, forsterite is the major contributing minerals for CO_2 mineralization. With increasing volume of forsterite from 0 to 0.0029 L (equivalent to 0.068 mol), the total mineralization increased from 1.08 to 8.37 mmol/L. This means that only 1.08 mmol/L carbonate mineralization was from anorthite, fayalite, and diopside, which contributed only 8.4% of total amount of mineralization (total amount of mineralization is 12.89 mmol/L). Forsterite is therefore a major contributing mineral to the in-situ CO_2 mineralization.

Collectively, a basalt reservoir deeper than 600 m, temperature below 50 °C, alkaline brine, and high percentage of forsterite was recommended as a "sweet" potential site to implement in-situ CO_2 mineralization. This investigation provided a pipeline to utilize geochemical modelling to find a potential reservoir for in-situ CO_2 mineralization.

Acknowledgements

This study was funded by Permanent Carbon Locking Future Science Platform, CSIRO under OD-233488. Impossible without you (IWY) project at CSIRO is acknowledged for supporting Yongqiang Chen. We thank the constructive communications with David Kinniburgh (the author of PhreePlot).

Conflict of interest

The authors declare no competing interest.

References

Agartan, E., Trevisan, L., Cihan, A., et al. Experimental study on effects of geologic heterogeneity in enhancing dissolution trapping of supercritical CO_2. Water Resources Research, 2015, 51(3): 1635-1648.

Agency, I. E. Exploring Clean Energy Pathways: The Role of CO_2 Storage. Paris, French Republic, International Energy Agency, 2019.

Anchliya, A., Ehlig-Economides, C., Jafarpour, B. Aquifer management to accelerate CO_2 dissolution and trapping. SPE Journal, 2012, 17(3): 805-816.

Aradóttir, E. S. P., Sonnenthal, E. L., Björnsson, G., et al. Multidimensional reactive transport modeling of CO_2 mineral sequestration in basalts at the hellisheidi geothermal field, iceland. International Journal of Greenhouse Gas Control, 2012, 9: 24-40.

Bachu, S. Review of CO_2 storage efficiency in deep saline aquifers. International Journal of Greenhouse Gas Control, 2015, 40: 188-202.

Bentham, M., Kirby, M. CO_2 storage in saline aquifers. Oil & Gas Science and Technology, 2005, 60(3): 559-567.

Bradshaw, J., Bachu, S., Bonijoly, D., et al. CO_2 storage capacity estimation: Issues and development of standards. International Journal of Greenhouse Gas Control, 2007, 1(1): 62-68.

Charlton, S. R., Parkhurst, D. L. Modules based on the geochemical model phreeqc for use in scripting and programming languages. Computers & Geosciences, 2011, 37(10): 1653-1663.

Chen, L., Wang, M., Kang, Q., et al. Pore scale study of multiphase multicomponent reactive transport during CO_2 dissolution trapping. Advances in Water Resources, 2018, 116: 208-218.

Chen, Y., Saeedi, A., Quan, X. Interfacial interactions of CO_2-brine-rock system in saline aquifers for CO_2 geological storage: A critical review. International Journal of Coal Geology, 2023, 274: 104272.

Chen, Y., Sari, A., Mu, J., et al. Fluid-fluid interfacial effects in multiphase flow during carbonated waterflooding in sandstone: Application of X-ray microcomputed tomography and molecular dynamics. ACS Applied Materials & Interfaces, 2021, 13(4): 5731-5740.

Gasda, S. E., Nilsen, H. M., Dahle, H. K. Impact of structural heterogeneity on upscaled models for large-scale CO_2 migration and trapping in saline aquifers. Advances in Water Resources, 2013, 62: 520-532.

Gunnarsson, I., Aradóttir, E. S., Oelkers, E. H., et al. The rapid and cost-effective capture and subsurface mineral storage of carbon and sulfur at the carbfix2 site. International Journal of Greenhouse Gas Control, 2018, 79: 117-126.

Hannis, S., Lu, J., Chadwick, A., et al. CO_2 storage in depleted or depleting oil and gas fields: What can we learn from existing projects? Energy Procedia, 2017, 114: 5680-5690.

Hartmann, J., West, A. J., Renforth, P., et al. Enhanced chemical weathering as a geoengineering strategy to reduce atmospheric carbon dioxide, supply nutrients, and mitigate ocean acidification. Reviews of Geophysics, 2013, 51(2): 113-149.

Ji, Y., Madhav, D., Vandeginste, V. Kinetics of enhanced magnesium carbonate formation for CO_2 storage via mineralization at 200 °C. International Journal of Greenhouse Gas Control, 2022, 121: 103777.

Kanakiya, S., Adam, L., Esteban, L., et al. Dissolution and secondary mineral precipitation in basalts due to reactions with carbonic acid. Journal of Geophysical Research: Solid Earth, 2017, 122(6): 4312-4327.

Kelemen, P. B., Matter, J. In situ carbonation of peridotite for CO_2 storage. Proceedings of the National Academy of Sciences of the United States of America, 2008, 105(45): 17295-17300.

Kinniburgh, D., Cooper, D. Phreeplot: Creating Graphical Output with Phreeqc. UK Status, UK Centre for Ecology & Hydrology, 2011.

Klein, F., Bach, W., McCollom, T. M. Compositional controls on hydrogen generation during serpentinization of

ultramafic rocks. Lithos, 2013, 178: 55-69.

McGrail, B. P., Spane, F. A., Amonette, J. E., et al. Injection and monitoring at the wallula basalt pilot project. Energy Procedia, 2014, 63: 2939-2948.

Michael, K., Arnot, M., Cook, P., et al. CO_2 storage in saline aquifers i-current state of scientific knowledge. Energy Procedia, 2009, 1(1): 3197-3204.

Nilsen, H. M., Syversveen, A. R., Lie, K. A., et al. Impact of top-surface morphology on CO_2 storage capacity. International Journal of Greenhouse Gas Control, 2012, 11: 221-235.

Oelkers, E. H., Declercq, J., Saldi, G. D., et al. Olivine dissolution rates: A critical review. Chemical Geology, 2018, 500: 1-19.

Palandri, J. L., Kharaka, Y. K. A compilation of rate parameters of water-mineral interaction kinetics for application to geochemical modeling. National Energy Technology Laboratory, U.S. Geological Survey Open File Report, 2004-1068, 2004.

Parkhurst, D. L., Appelo, C. A. J. Description of input and examples for phreeqc version 3-A computer program for speciation, batch-reaction, one-dimensional transport, and inverse geochemical calculations, in Modeling Techniques, edited by D. L. Parkhurst and C. A. J. Appelo, US Geological Survey, Denver, CO, pp. 497, 2013.

Pearce, J., Raza, S., Baublys, K., et al. Unconventional CO_2 storage: CO_2 mineral trapping predicted in characterized shales, sandstones, and coal seam interburden. SPE Journal, 2022a, 27(5): 3218-3239.

Pearce, J. K., Dawson, G. W., Golding, S. D., et al. Predicted CO_2 water rock reactions in naturally altered CO_2 storage reservoir sandstones, with interbedded cemented and coaly mudstone seals. International Journal of Coal Geology, 2022b, 253: 103966.

Pogge von Strandmann, P. A. E., Burton, K. W., Snæbjörnsdóttir, S. O., et al. Rapid CO_2 mineralisation into calcite at the carbfix storage site quantified using calcium isotopes. Nature Communications, 2019, 10(1): 1983.

Raza, A., Glatz, G., Gholami, R., et al. Carbon mineralization and geological storage of CO_2 in basalt: Mechanisms and technical challenges. Earth-Science Reviews, 2022, 229: 104036.

Rosenbauer, R. J., Thomas, B., Bischoff, J. L., et al. Carbon sequestration via reaction with basaltic rocks: Geochemical modeling and experimental results. Geochimica et Cosmochimica Acta, 2012, 89: 116-133.

Saeedi, A., Rezaee, R., Evans, B. Experimental study of the effect of variation in in-situ stress on capillary residual trapping during CO_2 geo-sequestration in sandstone reservoirs. Geofluids, 2012, 12(3): 228-235.

Saldi, G. D., Schott, J., Pokrovsky, O. S., et al. An experimental study of magnesite precipitation rates at neutral to alkaline conditions and 100-200 °C as a function of pH, aqueous solution composition and chemical affinity. Geochimica et Cosmochimica Acta, 2012, 83: 93-109.

Schaef, H. T., McGrail, B. P., Owen, A. T. Basalt reactivity variability with reservoir depth in supercritical CO_2 and aqueous phases. Energy Procedia, 2011, 4: 4977-4984.

Snæbjörnsdóttir, S. Ó., Sigfússon, B., Marieni, C., et al. Carbon dioxide storage through mineral carbonation. Nature Reviews Earth & Environment, 2020, 1(2): 90-102.

Soltanian, M. R., Amooie, M. A., Gershenzon, N., et al. Dissolution trapping of carbon dioxide in heterogeneous aquifers. Environmental Science & Technology, 2017, 51(13): 7732-7741.

Underschultz, J., Boreham, C., Dance, T., et al. CO_2 storage in a depleted gas field: An overview of the CO_2CRC Otway Project and initial results. International Journal of Greenhouse Gas Control, 2011, 5(4): 922-932.

Zhang, Y., Hu, B., Teng, Y., et al. A library of basic scripts of reaction rates for geochemical modeling using PHREEQC. Computers & Geosciences, 2019, 133: 104316.

Zhong, Z., Chen, Y., Fu, M., et al. Role of CO_2 geological storage in China's pledge to carbon peak by 2030 and carbon neutrality by 2060. Energy, 2023, 272: 127165.